

Temperature effect on nanotwinned Ni under nanoindentation using molecular dynamic simulation

Xi He(何茜), Ziyi Xu(徐子翼), and Yushan Ni(倪玉山)
Citation: Chin. Phys. B, 2024, 33 (**1**): 016201. DOI: 10.1088/1674-1056/acf997
Journal homepage: http://cpb.iphy.ac.cn; http://iopscience.iop.org/cpb

What follows is a list of articles you may be interested in

Layer thickness dependent plastic deformation mechanism in Ti/TiCu dual-phase nano-laminates

Minrong An(安敏荣), Yuefeng Lei(雷岳峰), Mengjia Su(宿梦嘉), Lanting Liu(刘兰亭), Qiong Deng(邓琼), Haiyang Song(宋海洋), Yu Shang(尚玉), and Chen Wang(王晨)
Chin. Phys. B, 2023, 32 (**6**): 066201. DOI: 10.1088/1674-1056/acb48f

Strengthening and softening in gradient nanotwinned FCC metallic multilayers

Yuanyuan Tian(田圆圆), Gangjie Luo(罗港杰), Qihong Fang(方棋洪), Jia Li(李甲), and Jing Peng(彭静)
Chin. Phys. B, 2022, 31 (**6**): 066204. DOI: 10.1088/1674-1056/ac4cc6

Effects of helium implantation on mechanical properties of $(Al_{0.31}Cr_{0.20}Fe_{0.14}Ni_{0.35})O$ high entropy oxide films

Zhao-Ming Yang(杨朝明), Kun Zhang(张坤), Nan Qiu(裘南), Hai-Bin Zhang(张海斌), Yuan Wang(汪渊), Jian Chen(陈坚)
Chin. Phys. B, 2019, 28 (**4**): 046201. DOI: 10.1088/1674-1056/28/4/046201

Investigation of mechanical properties of twin gold crystal nanowires under uniaxial load by molecular dynamics method

Guo-Wei Zhang(张国伟), Zai-Lin Yang(杨在林), Gang Luo(罗刚)
Chin. Phys. B, 2016, 25 (**8**): 086203. DOI: 10.1088/1674-1056/25/8/086203

Effect of twin boundary on nanoimprint process of bicrystal Al thin film studied by molecular dynamics simulation

Xie Yue-Hong (谢月红), Xu Jian-Gang (徐建刚), Song Hai-Yang (宋海洋), Zhang Yun-Guang (张云光)
Chin. Phys. B, 2015, 24 (**2**): 026201. DOI: 10.1088/1674-1056/24/2/026201

Temperature effect on nanotwinned Ni under nanoindentation using molecular dynamic simulation

Xi He(何茜), Ziyi Xu(徐子翼), and Yushan Ni(倪玉山)†

Department of Aeronautics and Astronautics, Fudan University, Shanghai 200433, *China*

(Received 18 July 2023; revised manuscript received 27 August 2023; accepted manuscript online 14 September 2023)

Temperature effect on atomic deformation of nanotwinned Ni (nt-Ni) under localized nanoindentation is investigated in comparison with nanocrystalline Ni (nc-Ni) through molecular simulation. The nt-Ni exhibits enhanced critical load and hardness compared to nc-Ni, where perfect, stair-rod and Shockley dislocations are activated at $(1\bar{1}1)$, $(\bar{1}11)$ and $(11\bar{1})$ slip planes in nt-Ni compared to only Shockley dislocation nucleation at $(1\bar{1}1)$ and $(\bar{1}11)$ slip planes of nc-Ni. The nt-Ni exhibits a less significant indentation size effect in comparison with nc-Ni due to the dislocation slips hindrance of the twin boundary. The atomic deformation associated with the indentation size effect is investigated during dislocation transmission. Different from the decreasing partial slips parallel to the indenter surface in nc-Ni with increasing temperature, the temperature-dependent atomic deformation of nt-Ni is closely related to the twin boundary: from the partial slips parallel to the twin boundary ($\sim$ 10 K), to increased confined layer slips and decreased twin migration(300 K–600 K), to decreased confined layer slips and increased dislocation interaction of dislocation pinning and dissociation (900 K–1200 K). Dislocation density and atomic structure types through quantitative analysis are implemented to further reveal the above-mentioned dislocation motion and atomic structure alteration. Our study is helpful for understanding the temperature-dependent plasticity of twin boundary in nanotwinned materials.

Keywords: nanoindentation, twin boundary, plastic deformation, molecular dynamics simulation

PACS: 62.20.F–, 61.72.Mm, 02.70.Ns, 68.35.bd **DOI:** 10.1088/1674-1056/acf997

1. Introduction

Nanocrystalline metals exhibit elevated strength with reduced plasticity. The dislocation interactions are the main plastic mechanism.[1,2] Nanotwinned metals with introduced twin boundary defects perform ultrahigh strength and extraordinary ductility,[3–5] which attracts great attention. The introduced twin boundaries exhibit the block of dislocation slip and act as dislocation nucleation sites during plastic deformation. Lu *et al.* proposed that the nanotwinned Cu achieves higher yield strength when the twin boundary spacing decreases, while a softening behavior appears when the twin boundary spacing is less than 15 nm.[6] Furthermore, Mousavi *et al.* discovered that there exists a softening temperature, below which the nanotwinned Cu hardens continuously as the twin spacing is reduced.[7] It is shown that mechanical behaviors and plastic deformation of nanotwinned metals are strongly influenced by temperature.

Recently, the temperature effect on the twin boundary was investigated. Zhao *et al.* reported that the nanotwinned Ti at a low temperature of 77 K can display elevated strength and enhanced ductility.[8] Larranaga *et al.* explored the high-temperature plasticity at the twin boundary in Al through straining experiments.[9] Shabib *et al.* credited that the twin migration process becomes faster and dislocation storage capacity is reduced at higher temperatures in the tensile experiment of 2D-columnar nanotwinned Cu films.[10] Huang *et al.* simulated the uniaxial tensile loading at different temperatures of nanotwinned Mg and found that temperature has a significant effect on the dislocation slip mechanism in the plastic deformation stage.[11] The shear loading simulation on nanotwinned Cu revealed that the deformation mechanism changes from the twin migration to deformation twinning with increasing temperature.[12] The above-mentioned studies of temperature effect of nanotwinned metals on microstructure deformation focus on uniform tension, compression, and shear load.

The localized indentation loading of nanoindentation is a method to investigate the mechanical responses and deformation mechanisms of films through experiments and simulations. The nanoindentation simulation is often used to investigate the atomic deformation of FCC nanotwinned materials including twinning, detwinning, and twin migration under room temperature.[13–16] The nanoindentation experiments about the temperature effect on FCC nanotwinned materials focus on mechanical behaviors of hardness,[17–19] and strain rate sensitivity.[2] Yang *et al.* revealed a large temperature-dependent increase in strain rate sensitivity and decrease in hardness through the nanoindentation experiment on nanotwinned Cu.[2] Yang *et al.* found that the strain rate of nanotwinned Cu is a function of temperature and hardness through multi-temperature indentation creep experiments.[17]

However, the twin boundary strengthening and the microstructure evolution of nanotwinned Ni with the increasing temperature under nanoindentation have not yet been explored

†Corresponding author. E-mail: niyushan@fudan.edu.cn

© 2024 Chinese Physical Society and IOP Publishing Ltd

via molecular dynamic simulation. Nickel (Ni) is one of the most technologically important high-temperature FCC metals, which has high temperature stability, high strength, and wear resistance. This paper investigates the atomic deformation of nanotwinned Ni (nt-Ni) to explain the mechanical properties in comparison with nanocrystalline Ni (nc-Ni) at five temperatures (10 K, 300 K, 600 K, 900 K, and 1200 K) under nanoindentation. The mechanical properties of critical loads, hardness, and indentation size effect of nt-Ni are analyzed through atomic deformation of incipient plasticity and dislocation transmission in comparison with nc-Ni. In addition, the evolution of atom types and dislocation density of nt-Ni are further studied to quantify atomic structure changes at various temperatures in comparison with nc-Ni. This study reveals the evolution of deformation mechanisms of high-strength nt-Ni at different temperatures, providing a theoretical basis for manufacturing and use of nt-Ni.

2. Simulation models and methods

In order to better investigate atomic structures of nc-Ni and nt-Ni under nanoindentation at different temperatures, the nc-Ni and nt-Ni films are established in a three-dimensional Cartesian coordinate system, as shown in Figs. 1(a) and 1(b). The size of the model is 18.92 nm × 20.69 nm × 9.75 nm, which is large enough to eliminate boundary effects for the indentation depth in our simulation. The size is coincident with the as-deposited nanotwinned Ni specimen for an average grain size value of 28 nm.[20] There are 357504 Ni atoms contained in the nc-Ni and nt-Ni models, which is enough to analyze the atomic deformation of nc-Ni and nt-Ni at different temperatures during the indentation process. To avoid potential boundary effects as a result of the small simulation dimensions of nc-Ni and nt-Ni, periodic boundary conditions are applied along the x and y directions so that the simulation box is replicated throughout the space to form an infinity lattice. The boundary condition of the z direction is set as free boundary conditions to realize the indentation process along the z direction. The nc-Ni in Fig. 1(a) has the lattice orientations along the x, y and z axes in $[1\bar{1}0]$, $[11\bar{2}]$ and $[111]$ directions. For the nt-Ni [Fig. 1(b)], two twin boundaries are introduced into the film by setting different lattice orientations. The lattice orientations of the 1st and 3rd layers in the x, y and z axes are along $[1\bar{1}0]$, $[11\bar{2}]$ and $[111]$. The lattice orientations of the 2nd layer along the x, y and z axes are $[\bar{1}10]$, $[\bar{1}\bar{1}2]$ and $[111]$. Thus, the lattice orientations of the two regions next to the twin boundary are opposite and mirror symmetric. Two boundaries are placed at 3.14 nm and 6.29 nm below the surface individually. The twin spacing around 3 nm is frequently attributed in as-deposited nanotwinned Ni samples, which is enough for observing atomic structures.[4] All atoms of the nc-Ni and nt-Ni films whose z coordinates are less than 0.78 nm are fixed to prevent the rigid movement of the whole films along the z axis during the nanoindentation process.

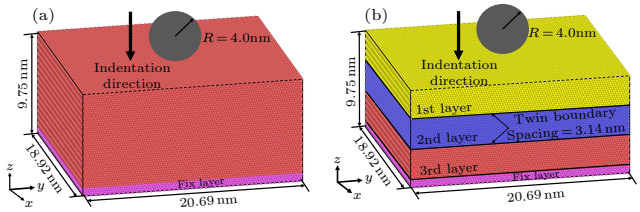


Fig. 1. Schematic representation of nanoindentation on (a) nc-Ni and (b) nt-Ni.

Table 1. The elasticity constants of Ni determined by Adam *et al.*, and EAM potential compared with the experimental data.[21,22]

	C_{11} (GPa)	C_{12} (GPa)	C_{44} (GPa)
Simulation[23]	235.6	153.1	133.7
Experiment 1[21]	253	152	124
Experiment 2[22]	247	147	125

The nanoindentation simulations are performed by using the large-scale parallel molecular dynamics package LAMMP[24] to examine the multiple mechanisms. A repulsive potential field is used to describe the force on each atom in contact with the indenter.[25,26] In this study, the embedded atom potential (EAM) method of Ni developed by Adams *et al.* is used to describe the interaction between Ni atoms.[23]

The elasticity constants are very close to the experimental data (see Table 1), which provide good results in modeling crystal defects. The repulsive potential has been extensively validated in various loading conditions, including tensile[27,28] and shear.[29] In recent years, especially in indentation simulation,[30–32] researchers have achieved good results in capturing stress responses, atomic deformations of Ni across different temperature ranges:[33–37]

$$V(r) = \begin{cases} k(R-r)^3, & r \leqslant R, \\ 0, & r > R, \end{cases} \tag{1}$$

where k is the contact stiffness, which is set to 10 eV·Å^{-3}, r is the distance between the atom and the center of the indenter, and R is the radius of the indenter. The lattice constant of single Ni (a_{Ni}) is 0.3520 nm. The spherical rigid indenter with radiation of 4 nm is used. The simulations are performed under five temperatures, namely 10 K, 300 K, 600 K, 900 K, and 1200 K. The time step is set to 1 fs. In each simulation, firstly the velocity of the movable atom is initialized and set randomly at the corresponding temperature. Then the whole film is subjected to 100000 steps of temperature relaxation in the isothermal-isobaric (NPT) ensemble to reach the set temperature, in which the total number of atoms, pressure, and temperature of the film remain unchanged. Then, the indentation is carried out along z-axis with a constant velocity of 10 m/s under the canonical (NVT) ensemble, in which the total number of atoms, the volume, and the temperature of the film remain unchanged. The visualization is performed by using OVITO.[38,39]

3. Results

3.1. Temperature effect on critical load

To learn the temperature influence on critical load during nanoindentation, we present the load responses (P–h) of nc-Ni and nt-Ni at the temperatures 10 K, 300 K, 600 K, 900 K, and 1200 K, as shown in Figs. 2(a) and 2(b). The simulation results of nc-Ni demonstrate the similar trend as the load response of nc-Ni indentation experiment.[40–43] The yield points of nc-Ni and nt-Ni in the P–h responses are labeled as A, B, C, D, E [Fig. 2(a)] and A′, B′, C′, D′, E′ [Fig. 2(b)], with the corresponding indenter depth and critical load, respectively, at 10 K, 300 K, 600 K, 900 K, and 1200 K. The yield points correspond to the onset of plasticity where dislocations nucleate from the indenter,[3] which is the critical point for the elastic-plastic transition beneath the indenter. Both the yield indenter depths and critical loads of nc-Ni and nt-Ni decrease with the increasing temperature, in agreement with past nanoindentation simulation results on nanocrystalline materials.[44] Although both the nt-Ni and nc-Ni yield at the similar indenter depth, the nt-Ni shows an elevated critical load compared with nc-Ni due to the existence of the twin boundary. The critical load difference between the nc-Ni and nt-Ni is presented in Fig. 3. Compared to nc-Ni, nt-Ni still has strengthening effect at high temperatures, especially at 300 K–900 K. Detailed atomic structures are presented in the next section.

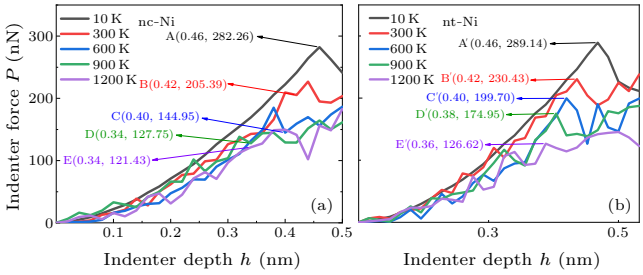


Fig. 2. Load-indenter depth responses at 10 K, 300 K, 600 K, 900 K, and 1200 K during nanoindentation of (a) nc-Ni and (b) nt-Ni.

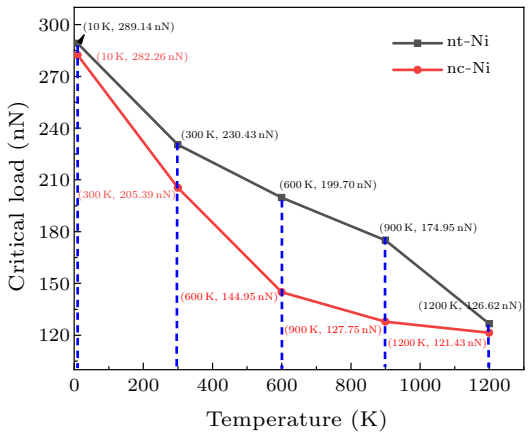


Fig. 3. Critical loads at 10 K, 300 K, 600 K, 900 K, and 1200 K of nc-Ni and nt-Ni.

3.2. Temperature effect on critical hardness

The hardness is a measure of a material's resistance to permanent deformation under an applied load.[45] In nanoindentation simulation, contact hardness H is defined as

$$H = \frac{P}{A_c}, \tag{2}$$

where P is the indenter force and A_c is the projected area of the contact surface between the indenter and the film along the direction z [111] (called the contact area). The projected area is calculated by[46]

$$A_c = \frac{\pi}{4}\left(x^{\max} - x^{\min}\right)\left(y^{\max} - y^{\min}\right). \tag{3}$$

Here, $x^{\max}$ and $x^{\min}$ are the maximum and minimum of x coordinates of atoms in contact with the indenter, $y^{\max}$ and $y^{\min}$ are the maximum and minimum of y coordinates of atoms in contact with the indenter.

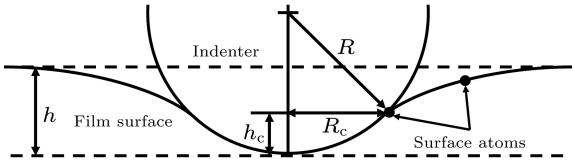


Fig. 4. Schematic diagram of the contact between the indenter and the film surface and surface atoms.

The hardness is generally considered to be correlated with contact depth h_c.[42] For the spherical indenters, at the same moment of indentation, the schematic diagram of h_c and h is shown in Fig. 4. The contact depth h_c is defined as

$$h_c = R - \sqrt{R^2 - R_c^2} = R - \sqrt{R^2 - \frac{A_c}{\pi}}. \tag{4}$$

The hardness–contact depth responses of nc-Ni and nt-Ni at various temperatures are shown in Figs. 5(a) and 5(b). The simulated results of nc-Ni demonstrate the trend similar to the hardness response of nc-Ni indentation experiment.[40–43] The results also align well with some nc-Ni indentation simulations.[47,48] The yield points of nc-Ni and nt-Ni in the H–h_c responses are labeled as A, B, C, D, E [Fig. 5(a)] and A′, B′, C′, D′, E′ [Fig. 5(b)], with the corresponding contact depth and critical hardness respectively at 10 K, 300 K, 600 K, 900 K, and 1200 K. Compared with the P–h curves, the hardness–contact depth response (H–h_c) offers insights into localized mechanical properties and exhibits trends that correspond to the material's microstructure, phase changes, and deformation mechanisms at different contact depths. The values of critical hardness of nc-Ni and nt-Ni decrease with the increasing temperature. Compared to nc-Ni, the nt-Ni shows a strengthening at all temperatures, as shown in Fig. 6. The tensile experiment response of yield strength with temperature on nt-Ti reported by by Zhao *et al.* also has the same decreasing variation tendency as our nanoindentation results.[8] The

above result is in accordance with the decreasing critical load responses with temperature, which indicates that nt-Ni still has strengthening effect at high temperature, especially at 300 K–900 K.

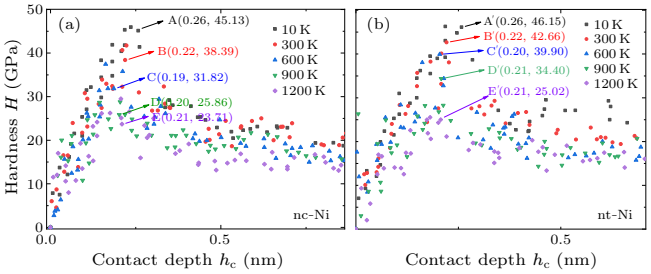


Fig. 5. Hardness–contact depth responses of (a) nc-Ni and (b) nt-Ni at 10 K, 300 K, 600 K, 900 K, and 1200 K during nanoindentation.

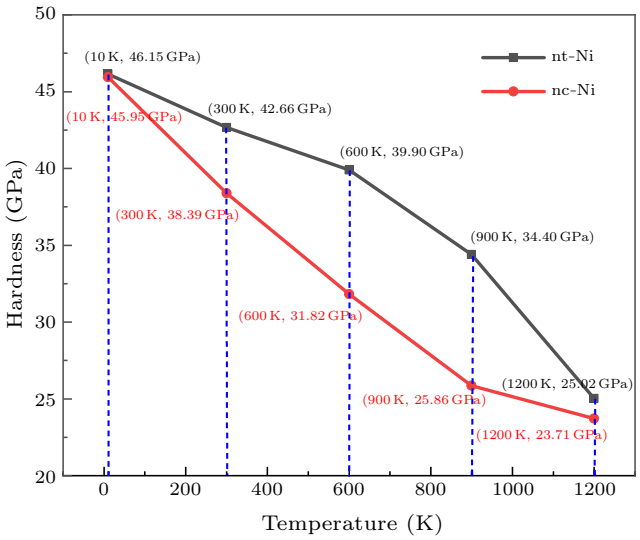


Fig. 6. The hardness difference between nc-Ni and nt-Ni.

3.3. Temperature effect on dislocation nucleation

Detailed atomic structure evolution could provide information about the underlying mechanisms of incipient plasticity corresponding to the yield event. The increased critical load and hardness are closely related to the atomic structures of nt-Ni.

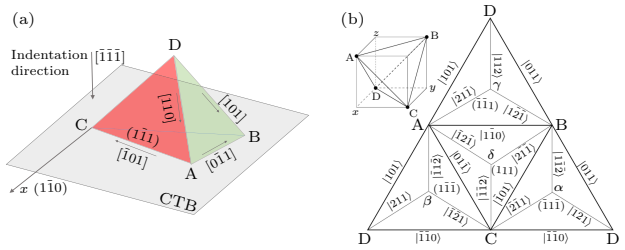


Fig. 7. (a) Thompson's tetrahedron illustrating the slips between the indenter surface and coherent twin boundary (CTB) in nt-Ni. (b) Thompson tetrahedron notation for FCC slip systems.

At the yield event, the dislocations are nucleated and emitted from the indented surface, followed by stacking faults, which correspond to the transition from elasticity to plasticity.[3] Figure 7 shows Thompson's tetrahedron illustrating the FCC slips. The dislocation types and slip planes at the yield point of nc-Ni and nt-Ni are presented in Fig. 8.

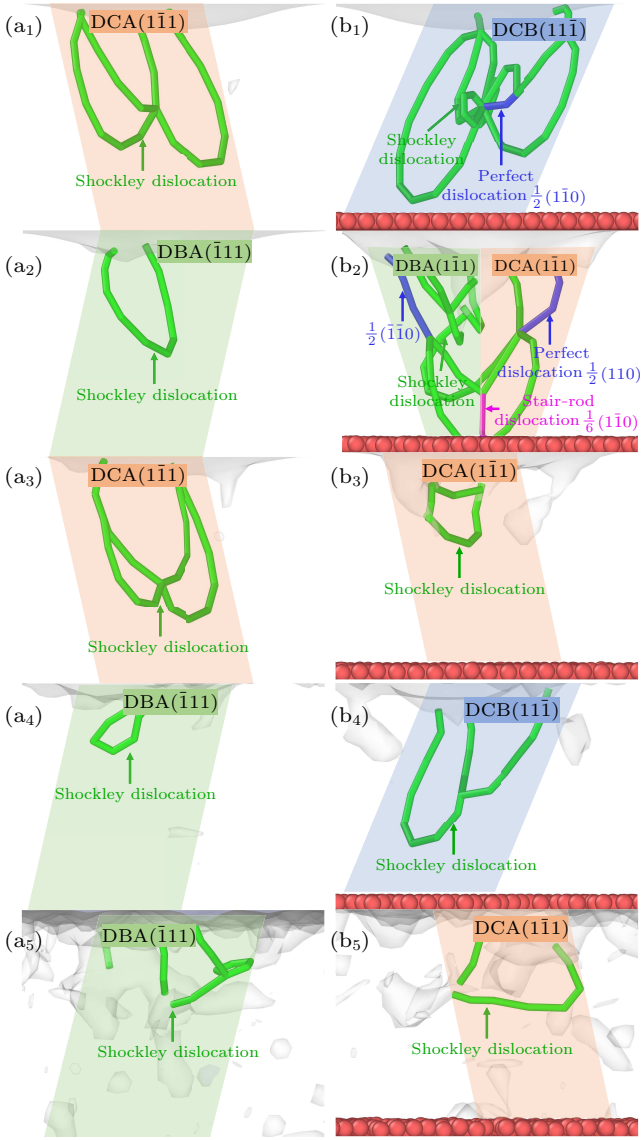


Fig. 8. The snapshots of the dislocation type and slips at the yield point of (a_1)–(a_5) nc-Ni and (b_1)–(b_5) nt-Ni at 10 K, 300 K, 600 K, 900 K, and 1200 K. The DCA, DCB, and DBA are the slip planes (refer to Thompson's tetrahedron in Fig. 7).

For nc-Ni at five temperatures [Figs. 8(a_1)–8(a_5)], only Shockley dislocations are generated at the yield point. The slip planes of $(1\bar{1}1)$ and $(\bar{1}11)$ are activated. For nt-Ni, at 10 K [Figs. 8(b_1)], perfect and Shockley dislocations are found in $(11\bar{1})$ slip plane. At 300 K [Fig. 8(b_2)], perfect, stair-rod and Shockley dislocations are observed in $(1\bar{1}1)$ and $(\bar{1}11)$ slip planes. The Shockley dislocations are found at the temperature of 600 K in $(1\bar{1}1)$ slip planes [Fig. 8(b_3)], 900 K [Fig. 8(b_4)] in $(11\bar{1})$ slip plane, and 1200 K in $(1\bar{1}1)$ slip plane [Fig. 8(b_5)]. Compared to nc-Ni, more active dislocations of perfect, stair-rod and Shockley dislocations nucleate and all slip planes of $(1\bar{1}1)$, $(\bar{1}11)$ and $(11\bar{1})$ are activated. The increased dislocation types and slip systems of nt-Ni are closely related to the

elevated stacking fault energy. The result indicates that active dislocation nucleation occurs and multiple slips are activated due to the impediment of the twin boundary in nt-Ni, which illustrates the strengthening of nt-Ni at different temperatures.

4. Discussion

4.1. Temperature effect on the indentation size effect of nt-Ni and nc-Ni

The characteristic of nanoindentation with an indenter is that the contact hardness decreases with contact depth. The well-established Nix–Gao model[18] is used to analyze the indentation size effect by the hardness responses, in which the hardness decreases with the increasing contact depth h_c after the yield points (onset of plasticity) in nc-Ni and nt-Ni. Based on geometrically necessary dislocations, this model can obtain the following relationship:

$$H = H_0\sqrt{1+\frac{h^*}{h_c}}, \tag{5}$$

where H is the hardness of the material under current indentation contact depth (h_c). H_0 is the macroscopic size-independent hardness at which H will converge to as the indentation depth becomes large enough (also called "infinite hardness"). Here, h^* is the characteristic indentation length scale depending on the microstructure of the material.[18] We fit the simulated hardness data with Eq. (5) using non-linear least squares, as shown in Figs. 9(a) and 9(b). The decreasing hardness of nc-Ni and nt-Ni with contact depth after the yield point can be well described using the Nix–Gao model. Both the hardness behaviors of nc-Ni and nt-Ni show an indentation size effect.

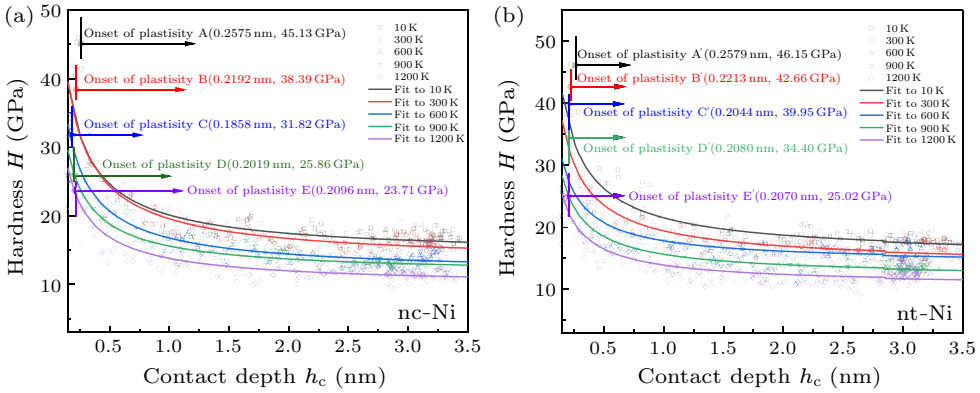


Fig. 9. Hardness–contact depth responses of (a) nc-Ni and (b) nt-Ni at 10 K, 300 K, 600 K, 900 K, and 1200 K during nanoindentation.

As is well known, h^* is the material length scale parameter, which is referred to the material-dependent plasticity length scale. According to Fleck and Hutchinson,[49] h^* characterizes the spacing between dislocation obstacles (in the case of pure metal, h^* represents the distance between other dislocations and their associated junctions and locks). In other words, h^* can be understood as the mean-free path of dislocation and reflects the magnitude of the indentation size effect.[50] The h^* values of nc-Ni and nt-Ni at different temperatures are shown in Fig. 10. Obviously, h^* of nc-Ni is greater than nt-Ni, indicating that the hardness of nc-Ni shows more significant indentation size effect compared to nt-Ni. Notably, h^* declines considerably in nc-Ni as the temperature rises, in agreement with nanoindentation results on nanocrystalline Cu.[50,51] Diversely, h^* in nt-Ni first declines and then increases as the temperature rises. The smaller h^* of nt-Ni indicates different dislocation nucleations and slips during plastic deformation in comparison with nc-Ni. It is desirable to explore the evolution of dislocation nucleation and propagation with the increasing temperature, which is studied in the following.

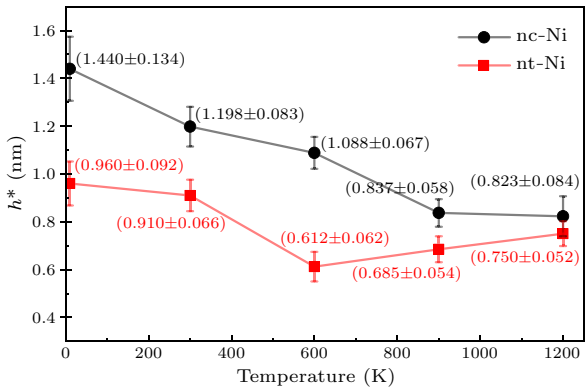


Fig. 10. Characteristic indentation length scale h^* of nc-Ni and nt-Ni at 10 K, 300 K, 600 K, 900 K, and 1200 K during nanoindentation.

4.2. Temperature effect on atomic deformation of nc-Ni and nt-Ni

It is known that the main plastic deformation mechanisms in FCC metals are dislocation cross-slip parallel or inclined to the surface, which will compete under different conditions. In this context, the twin boundary plays a crucial role in hindering the propagation of dislocations, as noted in the incipient plasticity analysis. The material length scale parameter h^* is

closed related to atomic deformation in the plastic stage.[52] To gain insight into the atomic deformation and the impediment effect of twin boundaries in nt-Ni under localized indentation loading at different temperatures, the dislocation transmission of nt-Ni is investigated in comparison with the corresponding atomic structures of nc-Ni, as shown in Fig. 11. After the yield point, the dislocation transmission is an important deformation mechanism between dislocations and twin boundaries in the plastic stage, where partial dislocations first are emitted from the upper twin boundary.[46] From Fig. 11, it can be found that in nc-Ni, the dominant deformation mechanism is dislocation slips and twinning, which are also observed in nanoindentation experiments of nc-Ni.[53,54] In nt-Ni, continuous emission of leading partial dislocations and trailing partial dislocations and steps along the twin boundaries are found, in align with observation in nanoindentation experiments of nt-Ni.[54]

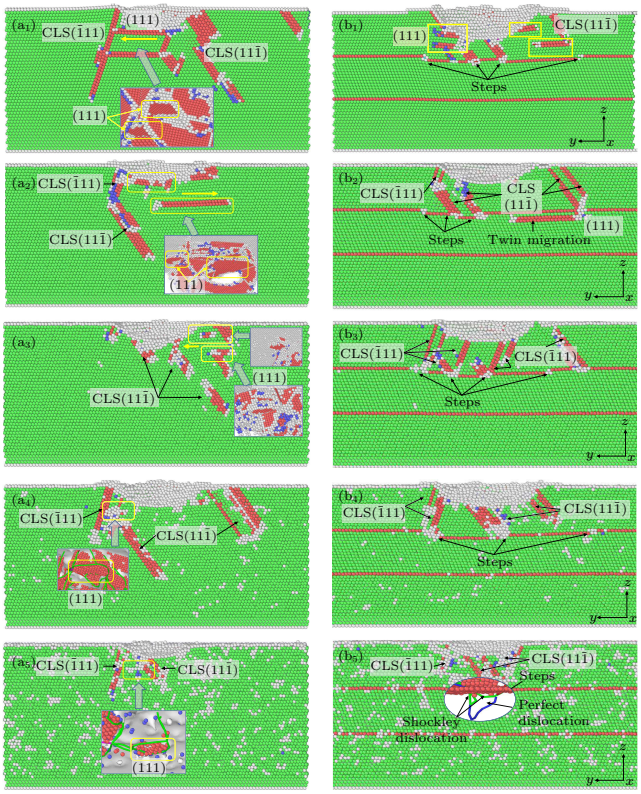


Fig. 11. Atomic structures of (a_1)–(a_5) nc-Ni and (b_1)–(b_5) nt-Ni when the dislocation transmission occurs in nt-Ni at 10 K (indenter depth h_{nt-Ni} = 1.94 nm), 300 K (indenter depth h_{nt-Ni} = 1.22 nm), 600 K (indenter depth h_{nt-Ni} = 1.34 nm), 900 K (indenter depth h_{nt-Ni} = 1.46 nm) and 1200 K (indenter depth h_{nt-Ni} = 0.88 nm). The CLS refers to the confined layer slips. The yellow rectangular boxes refer to the slip planes (111) parallel to the surface or twin boundary. The color of atom represents the local lattice structure of the atom, where green for FCC, red for HCP, blue for BCC, and gray for "other" lattice structures.

At 10 K, the atomic structures of nc-Ni and nt-Ni at the first dislocation transmission can be seen in Figs. 11(a_1) and 11(b_1). The dislocation slips are restrained because of the high activation energy acquired and dislocation block occurs in both nc-Ni and nt-Ni. In nc-Ni [Fig. 11(a_1)], two-layer partial slips parallel to the indented surface with the extension of stacking fault and multiple confined layer slips under the indenter surface are formed. Partial slips parallel to grain boundaries are pronounced at extremely low temperatures in nanocrystalline metals under nanoindentation, compression and tensile experiment.[55–59] The difference is that the confined layer slips and partial slips parallel to the indenter surface are only formed under the indenter due to concentrated loading and dislocation block. In nt-Ni [Fig. 11(b_1)], compared to nc-Ni, the dislocation propagation and the extension of stacking faults are impeded due to the twin boundary. Strengthening structures of multiple confined layer slips [($\bar{1}11$), ($1\bar{1}1$), ($11\bar{1}$)] between the indenter and the upper twin boundary are formed. At the same time, the partial twin migration acts as softening structure and steps on the twin boundary are the dislocation nucleation sources. The partial slips parallel to the twin boundary dominate the atomic deformation of nt-Ni at 10 K, which will soften the nt-Ni but improve the plasticity.[13] Figure 12 further reveals that great partial slips parallel to the twin boundary (111) dominate before dislocation transmission occurs, which will greatly delay the dislocation transmission event.

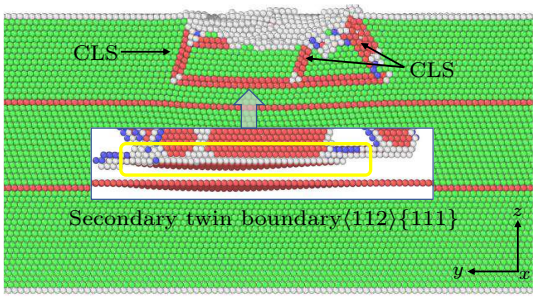


Fig. 12. Partial slips parallel to twin boundary in nt-Ni at 10 K, h = 1.22 nm. The CLS refers to the confined layer slips. The yellow rectangular boxes refer to the slip planes (111) parallel to the surface or twin boundary.

At 300 K, the dislocation slip is enabled in nc-Ni [Fig. 11(a_2)], partial slips parallel to the indented surface are still formed, while the range is smaller than that at 10 K. In nt-Ni [Fig. 11(b_2)], the dislocation block faded and no partial slips parallel to the twin boundary are formed, which greatly brings forward the dislocation transmission and decreases the plasticity. The confined layer slips between the indenter surface and twin boundary are formed. The twin migration and great dislocation nucleation steps on the twin boundary contribute to the plasticity of nt-Ni in comparison to that of nc-Ni.

Figure 11(a_3) illustrates a smaller range of partial slip parallel to the indenter surface in nc-Ni at 600 K in comparison with that at 300 K. In nt-Ni [Fig. 11(b_3)], compared to 300 K, more confined layer slips and less twin migration are found, which form strengthening structures under nanoindentation. In addition, more steps are formed on the twin boundary, which indicates the formation of more dislocation nucleation sites on the twin boundary and contributes to the elevated plasticity. It can be inferred that elevated temperature

promotes the interaction between dislocations, which is sufficiently flexible to allow the propagation of deformation along the slip planes.

In nc-Ni at 900 K [Fig. 11(a_4)], the decreased partial slips parallel to the indenter surface and increasing confined layer slips are formed compared to 600 K. Compared to 600 K, the nt-Ni at 900 K [Fig. 11(b_4)] has fewer confined layer slips and steps on the twin boundary, but it has a larger twin migration. Moreover, in nt-Ni at 900 K, the dislocation interaction of dislocation pinning and dissociation should be noted. Continuous dislocation lines are separated into several small dislocation segments [Fig. 13(a)], and then the separated dislocation segments are gathered to form dislocation pinning phenomena [Fig. 13(b)]. Dislocation dissociation and pining occur before the dislocation transmission at 900 K. On the one hand, the number of disordered atoms increases due to the enhancement of atomic thermal motion under high temperatures, which will hinder the motion of dislocations and separate the continuous dislocation line. On the other hand, the Shockley partial dislocations are emitted from the indented surface and interact with the stacking fault structure frequently due to the impediment of twin boundary and localized stress, resulting in dissociation and pinning of Shockley dislocations. This indicates that dislocation interaction occupies an important position and the strengthening effect of the twin boundary is decreased in the plastic deformation.

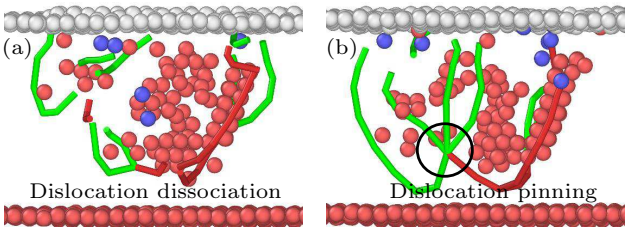


Fig. 13. (a) Dislocation dissociation ($h = 0.52$ nm) and (b) dislocation pinning ($h = 0.54$ nm) at 900 K.

In nc-Ni at 1200 K [Fig. 11(a_5)], the range of partial slips parallel to the indenter surface is narrowed and less confined layer slips are formed compared to those at 900 K. In nt-Ni [Fig. 11(b_5)], fewer confined layer slips in comparison with those of nt-Ni at 900 K, and no twin migration is observed. At the dislocation transmission point of nt-Ni, the dislocation loop directly traverses the upper twin boundary at the indenter depth of 0.88 nm. The perfect dislocation dissociates into three Shockley partial dislocations, two moving downward and one propagating transversely on the upper twin boundary. The phenomenon indicates the fading effect of the twin boundary hindering dislocation propagation. The dislocation interactions are also observed at 1200 K. Dislocation dissociation [Fig. 14(a)] and pining [Fig. 14(b)] are found to happen more frequently at 1200 K than at 900 K. It can be inferred that high temperature promotes the transition between the dislocation pining and dissociation. The result indicates that the strengthening effect of twin boundaries is reduced and dislocation interactions become the main deformation mechanism in nt-Ni at 1200 K.

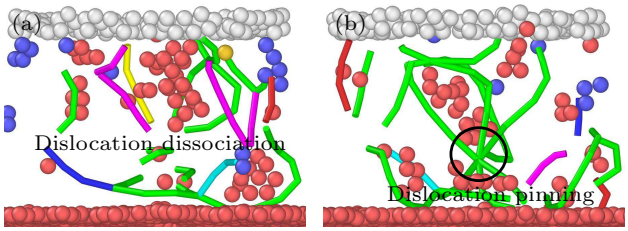


Fig. 14. (a) Dislocation dissociation ($h = 0.60$ nm) and (b) dislocation pinning ($h = 0.58$ nm) at 1200 K.

From the above analysis, it is found that compared to the downward extended dislocation slips in nc-Ni, the twin boundary of nt-Ni limits the dislocation nucleation and propagation to form a large amount of confined layer slips between the indenter surface and twin boundary at various temperatures. As the temperature increases, the dominant deformation of partial slips parallel to the indenter surface in nc-Ni decreases, which corresponds to the decrease of h^*. The deformation mechanism of nt-Ni that changes with the increasing temperature is different from that of nc-Ni. For nt-Ni, the changes of confined layer slip with the increasing temperature are in accordance with the change of h^*, which first decreases and then increases. The partial slips parallel to the twin boundary dominate the plasticity first. With the increasing temperature, the confined layer slips first increase and then decrease, which is helpful for the deformation propagation along slip planes. The dislocation interaction of dislocation pinning and dissociation then dominates the plastic deformation. It should be noted that the nt-Ni has strengthening structures at 300 K–900 K with multiple confined layer slips, great steps on the twin boundary and narrowed twin migration.

4.3. Quantitative analysis

4.3.1. Dislocation density of nc-Ni and nt-Ni

The dislocation density refers to the total length of dislocations contained in a unit volume crystal, or the number of dislocation lines crossing the unit cross-sectional area, which is closely related to dislocation motion. To complementally explain and analyze the dislocation motion at the dislocation transmission with temperature in nc-Ni and nt-Ni, the dislocation is calculated by the following formula:

$$\text{dislocation density} = \frac{L}{V},$$

where L is the total dislocation length, and V is the model volume. The continuous propagation of dislocations will lead to a pileup of dislocations, which will increase the strength of the material, and the dislocation densities of nc-Ni and nt-Ni vary at different temperatures, as shown in Fig. 15.

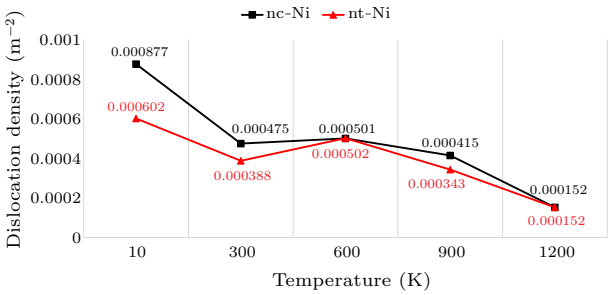


Fig. 15. Dislocation density of nc-Ni and nt-Ni when the dislocation transmission occurs in nt-Ni at 10 K (indenter depth $h_{\mathrm{nt-Ni}}$ = 1.94 nm), 300 K (indenter depth h = 1.22 nm), 600 K (indenter depth h = 1.34 nm), 900 K (indenter depth h = 1.46 nm), and 1200 K (indenter depth h = 0.88 nm).

It is shown that the dislocation density of nc-Ni is greater than that of nt-Ni because the twin boundary will hinder the propagation of dislocation and great dislocations are absorbed by the twin boundary. At 10 K, the dislocation slip is suppressed due to low stacking fault energy and then causes the increase of dislocation density. It can be observed that both nc-Ni and nt-Ni have high dislocation density at 10 K. The high dislocation density contributes lots to the formation of partial slip parallel to the indenter surface in nc-Ni [Fig. 11(a_1)] and nt-Ni [Figs. 11(b_1) and 12]. Dislocation density decreases in nc-Ni and nt-Ni at 300 K because of the decrease of dislocation block and activation of dislocation slips. Great atoms can obtain sufficient kinetic energy to break through the energy barrier to form inclined dislocation slips. It should be noted that the dislocation density of nt-Ni at 600 K is carried to a higher level and nearly identical to that of nc-Ni, which is consistent with the increased confined layer slip and steps on the upper twin boundary in the atomic structures in nt-Ni [Fig. 11(b_3)]. The elevated dislocation density contributes much to the increased plasticity in nt-Ni at 600 K. The dislocation density declines sharply because the dislocation pinning and dissociation are activated at 900 K [Figs. 13(a) and 13(b)] and 1200 K [Figs. 14(a) and 14(b)]. At 900 K and 1200 K, the difference in dislocation density between nc-Ni and nt-Ni decreases and becomes uniform, which indicates that the twin boundary gradually loses strengthening efficacy and the dislocation dominates plasticity of nt-Ni.

4.3.2. Atomic structures types of nc-Ni and nt-Ni

Atomic structure type change contributes a lot to the change of plastic structure such as confined layer slip, twinning, and twin migration under localized indentation loading. In order to further understand the plastic structure changes, the FCC atoms, disordered atoms and HCP atoms at the dislocation transmission points at five temperatures are calculated. The other atoms represent disordered atoms, and the number of other atoms indicates the intensity of the thermal motion of atoms. Greater disordered atoms indicate more violent atom thermal motion and cause softening. HCP atoms' attribution is closely related to the strengthening structures of nanotwinned materials under localized indentation loading. HCP atoms construct twin boundaries, twin migration, confined layer slips, and stacking faults in the nanotwinned materials under localized indentation loading. HCP atoms on twin boundaries, confined layer slips and stacking faults enhance nanotwinned materials, while HCP atoms on twin migration will lead to softening of the material.

The FCC atoms and disordered atom numbers of nc-Ni and nt-Ni with the temperature at the first dislocation transmission are presented in Figs. 16(a) and 16(b), respectively. It can be found that with the increasing temperature, the FCC atoms of both nc-Ni and nt-Ni decrease (Fig. 16(a)), while the disordered atoms increase with the increasing temperature (Fig. 16(b)). Moreover, fewer FCC atoms and more disordered atoms are found in nt-Ni compared with nc-Ni. The results reveal more active atoms motion and transformation happened in nt-Ni compared with nc-Ni due to the hindrance of the twin boundary. The attribution of HCP atoms in nc-Ni and nt-Ni is shown in Fig. 17 when the dislocation transmission occurs. In nt-Ni, the HCP atoms exist and construct the structures of confined layer slips and partial slips parallel to the indenter surface. The HCP atoms in nt-Ni are much greater than that in nc-Ni due to the existence of twin boundary. The HCP atoms in nc-Ni and nt-Ni decrease with the increasing temperature. This reveals that increasing temperature leads to changes in atomic structure of the twin boundary and stacking fault. Detailed HCP atoms attribution in nt-Ni is studied.

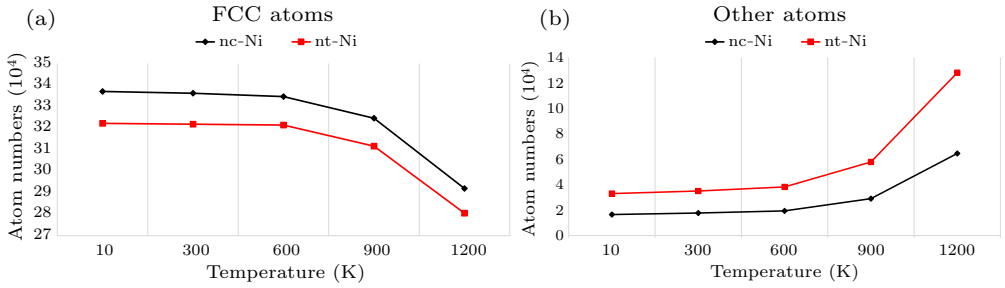


Fig. 16. (a) FCC atoms and (b) disordered atom ("other atoms" *in ovito*) number of nc-Ni and nt-Ni at 10 K, 300 K, 600 K, 900 K, and 1200 K when the dislocation transmission occurs in nt-Ni at 10 K (indenter depth $h_{\mathrm{nt-Ni}}$ = 1.94 nm), 300 K (indenter depth h = 1.22 nm), 600 K (indenter depth h = 1.34 nm), 900 K (indenter depth h = 1.46 nm), and 1200 K (indenter depth h = 0.88 nm).

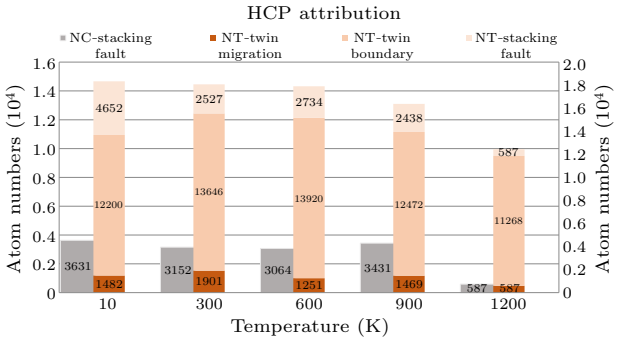


Fig. 17. HCP atom number and attribution of nc-Ni and nt-Ni at 10 K, 300 K, 600 K, 900 K, and 1200 K at the dislocation transmission when the dislocation transmission occurs in nt-Ni at 10 K (indenter depth $h_{\mathrm{nt-Ni}} = 1.94$ nm), 300 K (indenter depth $h = 1.22$ nm), 600 K (indenter depth $h = 1.34$ nm), 900 K (indenter depth $h = 1.46$ nm), and 1200 K (indenter depth $h = 0.88$ nm).

At 10 K, the stacking fault atoms (4652, 24.5%) are the largest among all temperatures, which corresponds to the partial slips parallel to the twin boundary and confined layer slips [Figs. 11(b_1) and 12]. At 300 K, the stacking fault atoms among HCP atoms occupy 13.9% (2527), smaller than that of nt-Ni at 10 K. However, the atoms participating in twin migration is 10.5% (1901) [Fig. 11(b_2)], larger than nt-Ni at 10 K. The change of HCP atoms indicates the softening of 300 K, compared to that at 10 K. At 600 K, 16.1% (2734) stacking fault HCP atoms are found, which is larger than that at 300 K. There is 7.4% (1251) of twin migration atoms that are recorded, which is smaller than that at 300 K. The HCP attribution is in good agreement with the atomic structures of nt-Ni at 600 K [Fig. 11(b_3)]. The HCP attribution can effectively mitigate the softening caused by increasing temperature. Compared to 600 K, the stacking fault HCP atoms of nt-Ni at 900 K decrease (2438, 14.6%) but twin migration HCP atoms increase (1469, 8.8%), so causing the reduction of confined layer slip in Fig. 11(b_4). At 1200 K, the stacking fault atoms of nt-Ni have a substantial reduction (587, 4.5%) without no twin migration, as shown in Fig. 11(b_5). The quantitative analyses of dislocation density and atomic structure on the one hand elaborate that the strengthening of nt-Ni at different temperatures is attributed to twin boundaries and confined layer slips, and on the other hand further illustrate that the atomic deformation of nt-Ni is changed with the increasing temperature during dislocation transmission.

5. Conclusion

In this paper, the atomic deformation of nt-Ni with twin boundaries at different temperatures under nanoindentation is investigated in comparison with nc-Ni. The results are as follows.

(i) Elevated critical load and hardness are found in nt-Ni compared to nc-Ni at the onset of plasticity due to the hindrance of twin boundary, where perfect, stair-rod, and Shockley dislocations are activated at $(1\bar{1}1)$, $(\bar{1}11)$, and $(11\bar{1})$ slip systems in nt-Ni compared to only Shockley dislocation nucleation at $(1\bar{1}1)$ and $(\bar{1}11)$ slip planes of nc-Ni.

(ii) Less significant indentation size effect is found in nt-Ni compared with nc-Ni in the plastic stage since twin boundaries hinder dislocation nucleation and propagation. The atomic deformation associated with the indentation size effect changes with the increasing temperature. Different from the decreasing dislocation slips in nc-Ni, the atomic deformation of nt-Ni changes as temperature rises: from the great partial slips and expansion parallel to the twin boundary dominate the plasticity ($\sim$ 10 K), to the great confined layer slips and decrease twin migration contribute to the (300 K–600 K), to the decrease of confined layer slips with the dislocation interaction of dissociation and pinning (900 K–1200 K).

(iii) Dislocation density and atom types through quantitative analysis further reveal the dislocation motion of dislocation slip and dislocation block and explain the atomic structure change of confined layer slip, stacking fault and twin migration. The strengthening structures of nt-Ni are attributed to twin boundaries and confined layer slips, which change as the temperature rises.

Acknowledgment

This work was supported by the National Natural Science Foundation of China (Grant No. 11572090).

References

[1] Shan Z, Stach E A, Wiezorek J M K, Knapp J A, Follstaedt D M and Mao S X 2004 *Science* **305** 5684
[2] Yang L W, Wang C Y, Monclús M A, Lu L, Molina-Aldareguía J M and Llorca J 2018 *Scr. Mater.* **154** 54
[3] Li X Y, Wei Y J, Lu L, Lu K and Gao H J 2010 *Nature* **464** 877
[4] Lu K, Lu L and Suresh S 2009 *Science* **324** 349
[5] Zhou H F, Li X Y, Qu S X, Yang W and Gao H J 2014 *Nano Lett.* **14** 5075
[6] Lu N D, Du K, Lu L and Ye H Q 2015 *Nat. Commun.* **6** 7648
[7] Taheri M S M, Zhou H F, Zou G J and Gao H J 2019 *npj Comput. Mater.* **5** 2
[8] Zhao S T, Zhang R P, Yu Q, Ell J, Ritchie R O and Minor A M 2021 *Science* **373** 1363
[9] Larranaga M, Lartigue-Korinek S, Legros M, Combe N and Mompiou F 2023 *Acta Mater.* **251** 118877
[10] Shabib I and Miller R 2009 *Model. Simul. Mater. Sci. Eng.* **17** 055009
[11] Huang K X, Yao J P, Hu Q Y, Shao L T and Sun Z 2019 *IOP Conf. Ser.: Mater. Sci. Eng.* **484** 012018
[12] Sinha T and Kulkarni Y 2011 *J. Appl. Phys.* **109** 114315
[13] Fu T, Peng X H, Chen X, Weng S Y, Hu N, Li Q B and Wang Z C 2016 *Sci. Rep.* **6** 35665
[14] Liu Y, Jian J, Chen Y X, Wang H Y and Zhang X H 2014 *Appl. Phys. Lett.* **104** 231910
[15] Li L and Ortiz C 2014 *Nat. Mater.* **13** 501
[16] Brons J G, Hardwick J A, Padilla H A, Hattar K, Thompson G B and Boyce B L 2014 *Mater. Sci. Eng. A* **592** 182
[17] Yang X S, Zhai H R, Ruan H H, Shi S Q and Zhang T Y 2018 *Int. J. Plast.* **104** 68
[18] Nix W D and Gao H J 1998 *J. Mech. Phys. Solids* **46** 411
[19] Manika I and Maniks J 2006 *Acta Mater.* **54** 2049
[20] Duan F H, Lin Y, Pan J, Zhao L, Guo Q, Zhang D and Li Y 2021 *Sci. Adv.* **7** eabg5113
[21] Ledbetter H M and Naimon E R 1974 *J. Phys. Chem. Ref. Data* **3** 897
[22] Mishin Y, Farkas D, Mehl M J and Papaconstantopoulos D A 1999 *Phys. Rev. B* **59** 3393

[23] Adams J B, Foiles S M and Wolfer W G 1989 *J. Mater. Res.* **4** 102
[24] Plimpton S 1995 *J. Comput. Phys.* **117** 1
[25] Baskes M I 1987 *Phys. Rev. Lett.* **59** 2666
[26] Baskes M 1992 *Physical Review B* **46** 2727
[27] Andric P and Curtin W 2017 *J. Mech. Phys. Solids* **106** 315
[28] Yin S, Cheng G M, Zhu Y and Gao H J 2020 *Phys. Rev. Mater.* **4** 023603
[29] Curnan M T, Shin D, Saidi W A, Yang J C and Han J W 2022 *Acta Mater.* **226** 117635
[30] Landman U, Luedtke W, Burnham N A and Colton R J 1990 *Science* **248** 454
[31] Sahputra I H 2021 *Eur. Phys. J. B* **94** 237
[32] Zhang J, Liu C, Shu Y H and Fan J 2012 *Appl. Surf. Sci.* **261** 690
[33] Wagih M, Larsen P M and Schuh C A 2020 *Nat. Commun.* **11** 6376
[34] Wolf D 2001 *Curr. Opin. Solid State Mater. Sci.* **5** 435
[35] Simonnin P, Schreiber D K and Rosso K M 2021 *Mater. Today Commun.* **26** 101982
[36] Keblinski P and Yamakov V 2003 *Interface Sci.* **11** 111
[37] Zhang J, Liu C and Fan J 2013 *Appl. Surf. Sci.* **276** 417
[38] Stukowski A 2010 *Model. Simul. Mater. Sci. Eng.* **18** 015012
[39] Stukowski A and Albe K 2010 *Model. Simul. Mater. Sci. Eng.* **18** 085001
[40] Jayaganthan R, Mohankumar K and Tay A A O 2005 *Int. J. Nanosci.* **4** 197
[41] Zhang X F, Fujita T, Pan D, Yu J S, Sakurai T and Chen M W 2010 *Mater. Sci. Eng. A* **527** 2297
[42] Zong Z, Lou J, Adewoye O O, Elmustafa A, Hammad F and Soboyejo W 2007 *Mater. Manufact. Processes* **22** 228
[43] Voyiadjis G Z and Yaghoobi M 2017 *Crystals* **7** 321
[44] He G C, Xu C, Liu C, Liu H P and Wang H K 2019 *Appl. Surf. Sci.* **480** 349
[45] Swain M V 1998 *Materials Science and Engineering* **253** 160
[46] Hu X W, Ni Y S and Zhang Z L 2020 *Nanomaterials* **10** 221
[47] Yan Y P, Zhou S R and Liu S 2017 *Comput. Mater. Sci.* **130** 16
[48] Imran M, Hussain F, Rashid M and Ahmad S A 2012 *Chin. Phys. B* **21** 116201
[49] Norman F and John W H 2001 *J. Mech. Phys. Solids* **49** 2245
[50] Franke O, Trenkle J C and Schuh C A 2010 *J. Mater. Res.* **25** 1225
[51] Chua Janel, Zhang R P, Chaudhari A, Vachhani S J, Kumar A S, Tu Q S and Wang H 2019 *Int. J. Mech. Sci.* **159** 459
[52] Petrík J, Blaško P, Mihaliková M, Vasilňáková A and Mikloš V 2019 *Metallurg. Res. Technol.* **116** 622
[53] TANG Bill T F, Zhou Y J, Zabev T, Brooks I and Erb U 2015 *J. Mater. Res.* **30** 3528
[54] Guo X K, Luo Z P, Li X Y and Lu K 2021 *Mater. Sci. Eng. A* **802** 140664
[55] Ahn D H, Kang M J, Park L J, Lee S and Kim H S 2017 *Mater. Sci. Eng. A* **684** 567
[56] Kappacher J, Tkadletz M, Clemens H and Maier-Kiener V 2021 *Materialia* **16** 101084
[57] Robinson J, Verma A, Homer E R and Thompson G B 2023 *Mater. Sci. Eng. A* **871** 144866
[58] Zhu Y T, Wu X L, Liao X Z, Narayan J, Mathaudhu S and Kecskes L 2009 *Appl. Phys. Lett.* **95** 031909
[59] Zhu Y T, Wu X L, Liao X Z, Narayan J, Kecskes L and Mathaudhu S 2011 *Acta Mater.* **59** 812